JOURNAL OF MATERIALS SCIENCE 30 (1995) 321–333

Thermal stability of Al_2O_3–5 vol % SiC nanocomposite

J. WANG, C. B. PONTON, P.M. MARQUIS
Materials Science Programme, Faculty of Science, National University of Singapore, Singapore

An alumina nanocomposite containing 5.0 vol % SiC, which exhibits a fracture toughness of more than three times that of conventional alumina ceramics, was fabricated by hot pressing a powder mixture consisting of submicrometre alumina and silicon carbide powder particles at temperatures in the range 1600–1700 °C. SiC particles, 20–30 nm in size, were observed to occur primarily at the intragranular positions in the alumina matrix. The nanocomposite was then thermally aged in air for various periods at 1400 °C. The thermal treatment led to the formation of a reacted surface scale, the thickness of which increases with increasing ageing time at the ageing temperature. The microstructure of the reacted surface scale was studied using XRD, SEM and TEM equipped with an EDX analysis facility. At the thermal ageing temperature, SiC particles within the surface scale are oxidized to form silica, which subsequently reacts with the alumina matrix. The oxidation of the SiC particles and the subsequent reaction with the alumina matrix, together with the grain growth of various phases, resulted in the formation of a porous microstructure, which consists of alumina grains, mullites of differing composition, and amorphous silica and aluminosilicate pockets. Two types of mullite phase, which contain a high and a low level of silica, respectively, were identified in the surface scales. The high silica-containing mullite phases, the composition of which is close to that of stoichiometric mullite, occur as large, irregularly shaped matrix grains. The low silica-containing mullite phases (15–20 wt % SiO_2), which exhibit a rounded morphology, are observed to occur as second-phase particles entrapped within the high-silica containing mullite grains. The nanocomposite structure in the bulk region remains almost intact when compared with that of the unaged nanocomposite. The only noticeable difference is that the alumina matrix in the thermally aged nanocomposite exhibits a slightly larger grain size than that of the unaged nanocomposite.

1. Introduction

Ceramic nanocomposites are a class of relatively new materials, which offer a better mechanical performance than conventional ceramic materials over a wide temperature range [1–4]. For example, Al_2O_3–SiC nanocomposites exhibit a fracture toughness of more than three times that of monolithic alumina, together with a much improved fracture strength at both room temperature and elevated temperatures. Following the early pioneering research work by some Japanese scientists, notably led by Niihara [1, 2, 4], there has been tremendous interest in developing and characterizing nanophase ceramic materials in the advanced ceramic community. By definition, a nanocomposite is a two or multi-phase system with structural features in the 1–50 nm size range and with at least one component being distributed in nanometre scales [5]. Three types of microstructure may therefore be categorized, including intergranular ceramic nanocomposites, intragranular ceramic nanocomposites and nano/nano ceramic composites. Most of the ceramic nanocomposites studied in the last few years involve SiC as a reinforcing phase and several SiC-containing systems, including the Al_2O_3–SiC, mullite-SiC, ZrO_2–SiC, MgO–SiC and Si_3N_4–SiC systems, have been exploited mainly for mechanical performance. A great research effort is being focused on the microstructure–mechanical property relationships in these nanophase materials, as many of the processing details given in the published work are sketchy and contradictory and the mechanism by which the mechanical properties are improved is unclear [3, 5].

For engineering applications at elevated temperatures, it is essential that the structural materials exhibit a microstructural stability against a desired thermal duration [6]. Many ceramic materials suffer a huge microstructural and, therefore, property degradation when subjected to a high-temperature treatment. The unwanted grain growth and cavitation at the grain boundaries and grain junctions in oxide ceramics results in the formation of a poor microstructure and the mechanical performance is rapidly deteriorated [7]. The failure of non-oxide ceramics, such as SiC, Si_3N_4, is often associated with the un-

0022–2461

desirable oxidation in an oxidizing atmosphere at the application temperatures [8, 9]. Therefore, the oxidation resistance of SiC ceramics has received a great deal of attention over the last three decades in the advanced ceramic community. Two types of oxidation behaviour have been identified: active and passive oxidations [10–13]. In a less oxidizing environment, the oxidation of silicon carbide grains results in the formation of gaseous species such as SiO and CO, which do not protect the material from further oxidation. The continuous oxidation, shown as a continuous weight loss, degrades the mechanical properties of SiC ceramics by introducing microstructural defects or reducing the load-bearing cross-section. In a highly oxidizing atmosphere such as in oxygen or in air, a dense silica layer is formed on the sample surface which acts as an effective protecting barrier against further oxidation. The oxidation rate, therefore, represented by either the weight gain or the scale thickness as a function of oxidation time, slows down with increasing oxidation time [8, 14]. A parabolic relationship between the scale thickness and oxidation time is observed, although the presence of sintering additives may lead to a degree of deviation [15, 16]. Oxidation of SiC whisker-reinforced alumina and mullite composites was first observed during mechanical testing at elevated temperatures and was studied by Kriven *et al.* [17]. They reported that the oxidation at temperatures above 700 °C resulted in a significant reduction in the room-temperature flexural strength of a 20 vol % SiC whisker-reinforced alumina composite. A reacted surface scale, which exhibited a poor microstructure and a mainly transgranular fracture surface, was observed to occur in the oxidized materials. The SiC whiskers within the surface scale were oxidized at the oxidation temperature, forming silica. The resultant structure consisted of alumina grains, amorphous silica pockets at the triple grain junctions and mullite grains, which are a reaction product between the alumina matrix and the silica [18, 19].

Alumina–SiC nanocomposite is a thermodynamically metastable system at elevated temperatures [20]. Similar to the conventional SiC ceramics and SiC whisker-reinforced ceramic composites, SiC particles in the nanocomposite, specially those near to the sample surface, are susceptible to oxidation at temperatures above 1000 °C, forming silica which may subsequently react with the alumina matrix. Therefore, a reacted surface scale is expected to form in the Al_2O_3–SiC nanocomposites when subjected to an oxidation in air at high temperatures. Furthermore, microstructural change, such as grain growth and cavitation at the grain boundaries, may occur in the bulk region of the aged nanocomposite although oxidation may not take place in this region. The aim of the present work was to investigate the response of an Al_2O_3–SiC nanocomposite when thermally aged at 1400 °C in air.

2. Experimental procedure

The Al_2O_3–SiC nanocomposite selected for the thermal stability study was fabricated using a well-established processing route, using commercially available alumina (CR15, Baikowski Chemie, Annecy, France) and silicon carbide (ENEA, Frascati, Italy) powders as the starting materials [3, 5]. The as-received alumina powder had an average particle size of 0.3 μm and silicon carbide powder an average particle size of 19 nm. Appropriate amounts of the alumina powder and silicon carbide powder, for the composition of Al_2O_3–5.0 vol % SiC, were mixed together by ball milling in isopropanol using zirconia balls as milling medium for 16 h. The milled powder suspension was dried on a hot plate. The Al_2O_3–SiC powder compact was densified at a temperature 1650 °C and a pressure of 20 MPa, resulting in a sintered density of 96.5 % theoretical density. The as-hot pressed nanocomposite sample, which had a dimension of 50 mm × 50 mm × 3 mm, was cut into bars of 50 mm × 8 mm × 2.5 mm. Thermal ageing was then carried out at 1400 °C in air for various periods from 0–90 h.

Both the thermally aged and unaged Al_2O_3–SiC nanocomposites were characterized for phases and microstructure. XRD phase analysis was employed to identify phases present in each material. Both the fracture and polished and then thermally etched surfaces were examined using scanning electron microscope (SEM, Joel-5200). An analytical TEM study, together with an energy dispersive analysis (EDX), were carried out on the nanocomposites thermally aged at 1400 °C for various periods. As will be discussed as follows, the thermally aged nanocomposites exhibited a sandwich-like structure: consisting of a reacted surface layer (scale) and the retained nanocomposite structure in the bulk region. As shown in Fig. 1, two types of TEM specimens were prepared for each thermally aged nanocomposite: from the reacted surface scale and from the bulk (central) region, respectively. For the reacted surface scale, a 150 μm thick slice was cut in the direction parallel to the sample surface, using a diamond slicing wheel. The slice was further reduced to an approximate 80 μm thickness by grinding the cut surface using 800 grit silicon carbide slurry. Discs, 3 mm diameter, were obtained from the slice, followed by further polishing

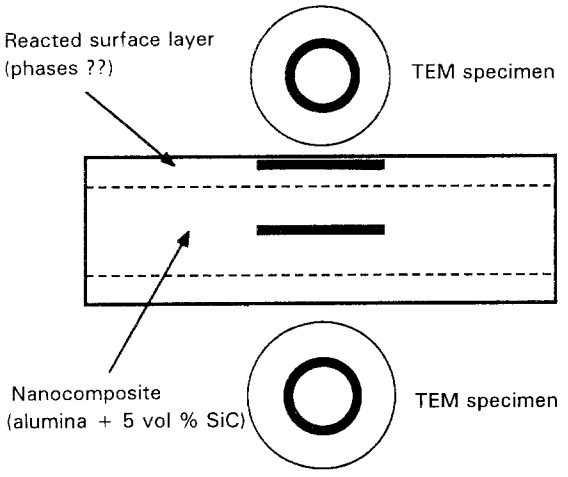

Figure 1 A schematic drawing showing that the thermally aged nanocomposites exhibit a sandwich-like structure. Two types of TEM specimen were prepared, from the reacted surface scale and from the retained nanocomposite in the bulk region, respectively.

on the cut surface side using a dimpler machine and then dimpling (Model 515, South Bay Technology Inc, CA). The thin foils were finally polished in an ion beam thinner (Gaton Model 600, Corby, UK) and coated with carbon. It was estimated that the distance between the region to be examined in TEM and the as-aged sample surface is approximately 10 μm. Thin foils from the bulk region of the thermally aged nanocomposites were prepared by following a similar route. The only difference was that the latter were prepared by reducing the foil thickness on both sides of the thin slice and then specimen discs. The analytical TEM study was carried out on both types of the thin foils using a Joel 4000CX equipped with an EDX facility, at an operation voltage of 300 kV.

3. Results and discussion

The as-hot pressed Al_2O_3–5.0 vol % SiC nanocomposite exhibited a black appearance, which is similar to other engineering ceramics fabricated via hot pressing in a graphite die. XRD phase analysis (CuK_α) indicated that it consisted of an α-alumina matrix and silicon carbide. Fig. 2a and b are two bright-field transmission electron micrographs showing the microstructure of the as-hot pressed Al_2O_3–5.0 vol % SiC nanocomposite. The conventional ball milling in propanol resulted in a mixed degree of dispersion uniformity of the SiC particles in the alumina matrix. On the one hand, most of the SiC particles are dispersed in and entrapped by the alumina grains. On the other hand, an estimated 20 % of the SiC particles are situated at the grain boundaries and grain junctions of the alumina matrix. These intergranularly positioned SiC particles formed particles agglomerates of 50–300 nm in sizes. Furthermore, the intragranularly positioned SiC particles are not uniformly distributed in the alumina matrix, although they do not form any degree of agglomeration. Specifically, the number of the engulfed SiC particles varies considerably from one alumina grain to another and a fraction of the alumina grains do not contain any SiC particles. Within each SiC-containing alumina grain, the dispersion of SiC particles is rarely uniform. Dislocation networks are shown to occur in many alumina grains containing SiC particles. However, certain SiC-containing alumina grains do not exhibit any dislocation networks. The SiC particles underwent little grain growth at the hot-pressing temperature, as indicated by their particle sizes (20–30 nm), compared to the average particle size of 19 nm of the as-received SiC powder. In fact, little necking was observed between neighbouring SiC particles within the SiC agglomerates at the triple grain junctions of the alumina matrix, implying that a large degree of densification was not occurring within these particle agglomerates at the hot-pressing temperature. The alumina matrix demonstrated a quite narrow grain-size distribution with the average grain size being 0.70 μm, as measured by the linear interception technique. Abnormal grain growth of the alumina matrix, up to 2 μm, was, however, found in the regions where few or no SiC particles are present. This indicates that the SiC particles acted as an effective grain-growth inhibitor for the alumina matrix at the hot-pressing temperature.

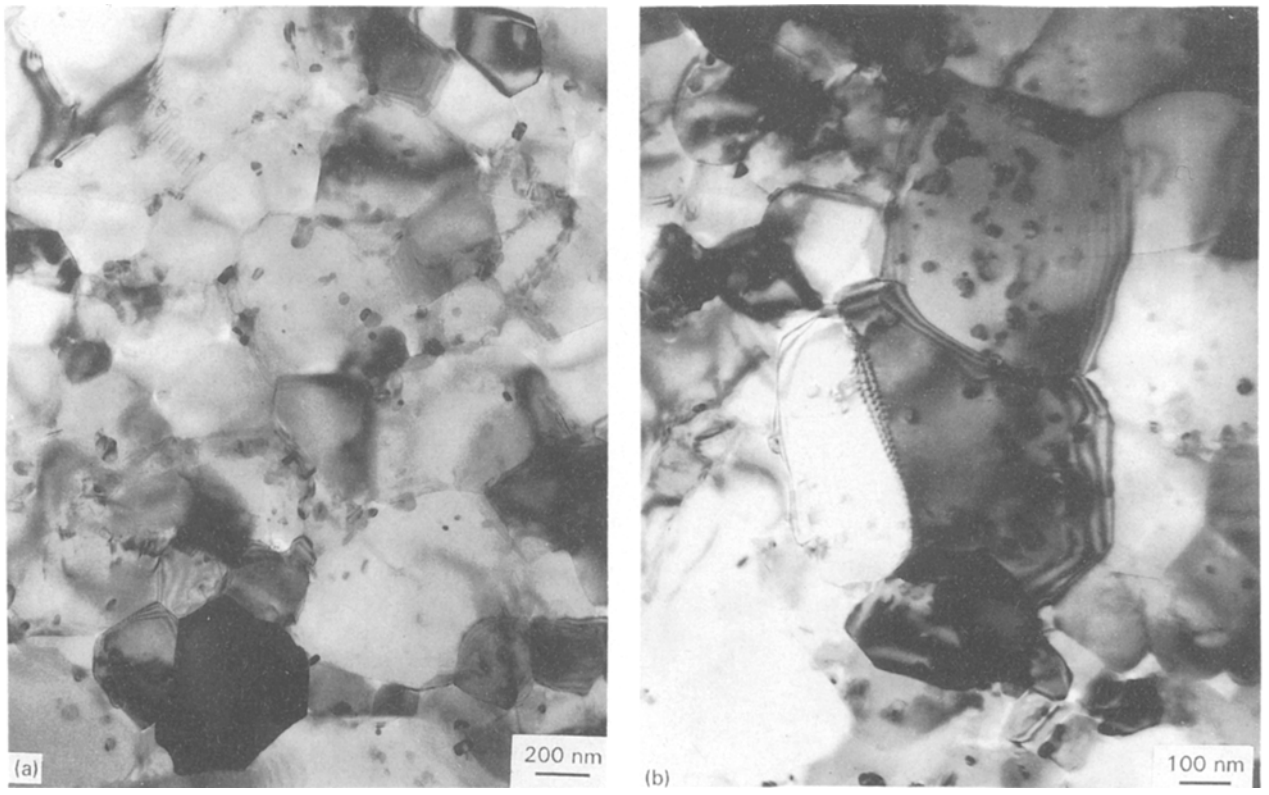

Figure 2(a, b) Two bright-field transmission electron micrographs showing the microstructure of the as-hot pressed Al_2O_3–5.0 vol % SiC nanocomposite. The conventional ball milling resulted in a mixed degree of mixing homogeneity of the SiC particles in the alumina matrix.

The as-hot pressed Al_2O_3–5.0 vol % SiC nanocomposite demonstrated improved mechanical properties over monolithic alumina matrix fabricated using an identical hot-pressing route. As an example, the former exhibits a three-point bend strength of 700 MPa and an indentation toughness of 10.3 MPa $m^{0.5}$, compared with a three-point bend strength of 300 MPa and an indentation toughness of 2.7 MPa $m^{0.5}$ for the latter. The presence of processing-related microstructural defects, such as lamination flaws which were observed to occur in the as-hot pressed materials, are responsible for the low fracture strength measured. As shown in Fig. 3, the fracture surface of the as-hot pressed nanocomposite is mainly transgranular. This agrees well with the fracture surface observed by Niihara and co-workers [1, 5] and Zhao and co-workers [3] in alumina–SiC nanocomposites.

On thermal ageing at 1400 °C in air, the black appearance of the as-hot pressed Al_2O_3–5.0 vol % SiC nanocomposite faded off quickly with increasing ageing time. For example, the nanocomposite is slightly faint with a few white spots on the surface when aged for 5 h. Both the density of the white spots and the size of each white spot increased with increasing ageing time. The thermally aged nanocomposite exhibited a white appearance when aged at 1400 °C for more than 15 h. XRD phase analysis showed that SiC disappeared from the aged surface and mullite emerged at the same time. Fig. 4a–d are scanning electron micrographs showing the sandwich-like structure of the thermally aged nanocomposites at 1400 °C for 8, 40, 55 and 90 h, respectively. There is a reacted surface scale, which has a different contrast to the retained nanocomposite inside, in each thermally aged material. It is also seen from these micrographs that crack-like pores occur in the reacted surface scales, especially in those of the thermally aged nanocomposites at 1400 °C for a long period. To illustrate further the poor microstructure of the reacted surface layer, Fig. 5a–c show scanning electron micrographs of the fracture surfaces of the thermally aged nanocomposites at 1400 °C for 8, 40 and 90 h, respectively. Unlike the microstructure of the retained nanocomposite in the bulk region, the reacted surface scales appear porous and do not show a mainly transgranular fracture surface. They also demonstrate a wider grain-size distribution and a more rounded grain morphology than the nanocomposite structure in the bulk region. More rounded grains were observed to occur in the nanocomposite aged for a longer period than that aged for a shorter period. Their fracture surfaces consist of both intragranularly fractured large grains and intergranularly fractured small grains.

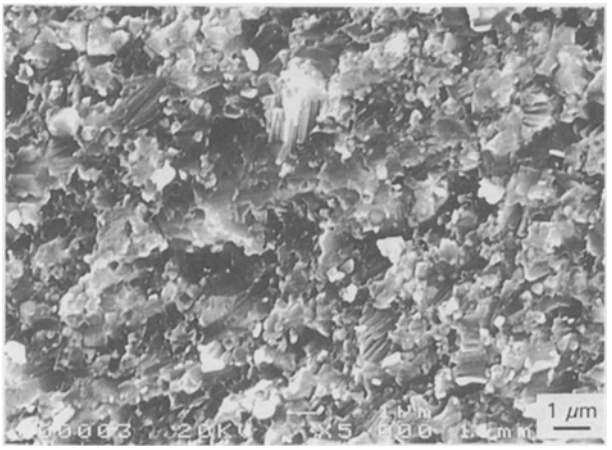

Figure 3 A scanning electron micrograph showing the primarily transgranular fracture surface of the as-hot pressed nanocomposite.

To establish the oxidation mechanism of SiC particles in the as-hot pressed Al_2O_3–5.0 vol % SiC nanocomposite, the thickness of the reacted surface scale versus ageing time is plotted in Fig. 6. Two parabolic stages are observed over the time range investigated in the present work from 0–90 h; (i) the thickness of the reacted surface scale increases dramatically with increasing ageing time from 0–2 h. The increase rate then slows down with a further increase, up to 15 h, in ageing time; (ii) the increase rate picks up again over the time range of 15–50 h, followed by a decrease in the increase rate when aged for more than 50 h. The increase rate in the scale thickness over the period of 2–90 h is much lower than the initial increase rate, although it goes up and down at the second parabolic stage. Therefore, the second parabolic stage may simply be regarded as a deviation from the first parabolic stage. It may thus be concluded that the oxidation of the Al_2O_3–5.0 vol % SiC nanocomposite at 1400 °C in air is a passive type [14, 15]. To support this conclusion further, a parabolic relationship between weight gain and ageing time was observed for the nanocomposite during a preliminary TGA study at 1400 °C in air.

As mentioned earlier, the passive oxidation rate is controlled by the diffusion rate of a particular gaseous species, either the inward diffusion of oxygen or the outward diffusion of product gases such as CO or CO_2, through the oxidation scale [10]. Both single-crystal and high-purity polycrystalline SiC ceramics demonstrate a single parabolic relationship between the surface scale thickness and ageing time in an oxidizing atmosphere, such as in air, at elevated temperature [8, 14]. The presence of a sintering additive phase or an impurity phase at the grain boundaries and grain junctions often results in the occurrence of multi-parabolic stages [21]. Specifically, the oxidation rate increases with the increasing amount of additive phase, due to the impact of the additive phase on the physical and structural characteristics of the surface scale and therefore on the diffusion rate of gaseous species through the surface scale [16, 22]. The scale thickness–ageing time relationship shown in Fig. 6 is very similar to the multi-parabolic stages observed by Maeda *et al.* [21] in a sintered Al_2O_3-containing polycrystalline SiC ceramic when subjected to a long-term oxidation. They attributed such behaviour to various microstructural changes in the surface scale, involving subsequential crystallization of the amorphous silica, phase transformation of the crystalline silica and viscosity change of the oxide scale due to migration of the sintering additives. It is therefore interesting to compare the experimental result shown in Fig. 6 with that of a polycrystalline SiC

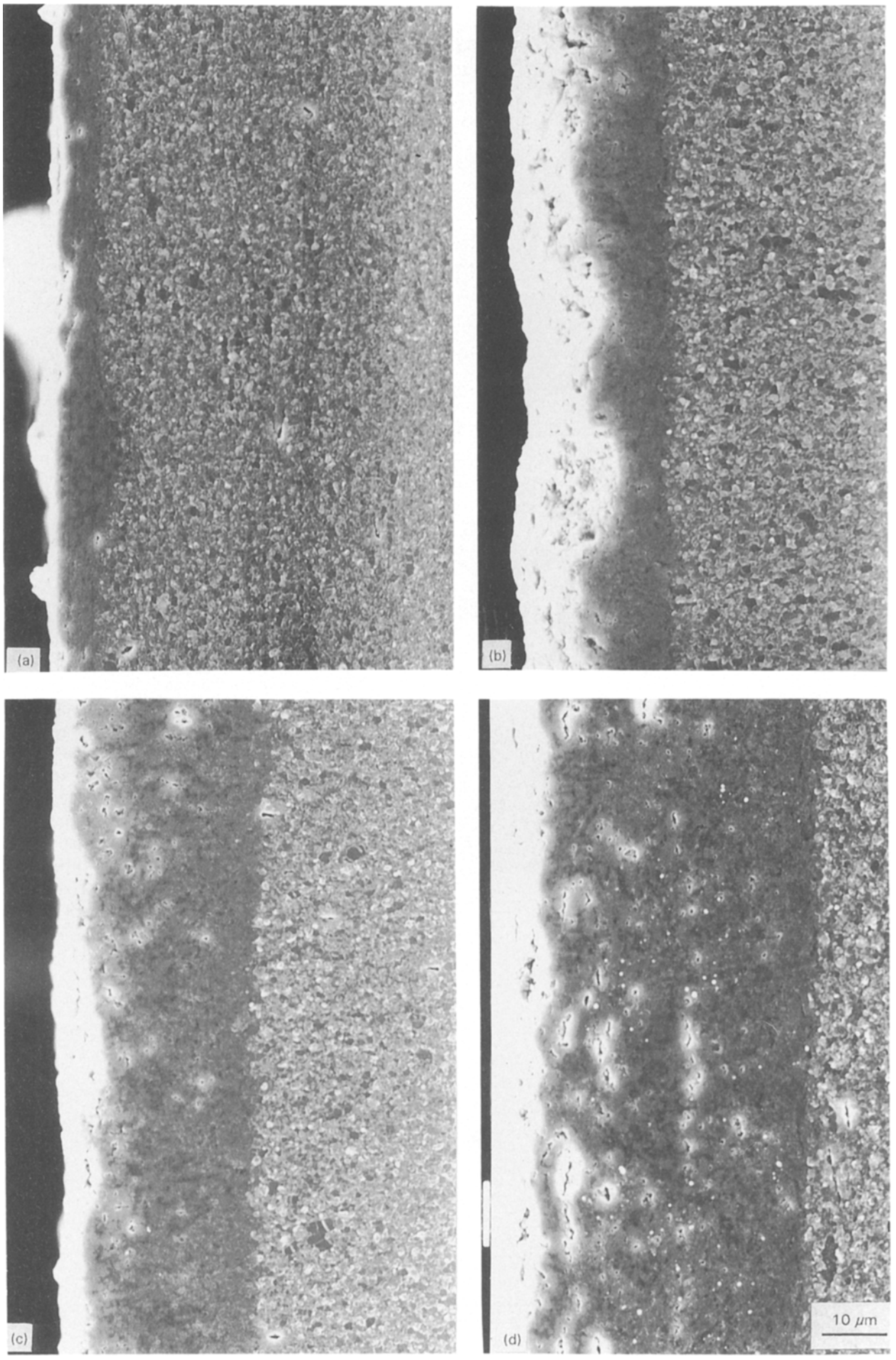

Figure 4 The sandwich-like structure of the thermally aged nanocomposites at 1400 °C for (a) 8, (b) 40, (c) 55 and (d) 90 h. The reacted surface scale has a different contrast to the retained nanocomposite structure inside.

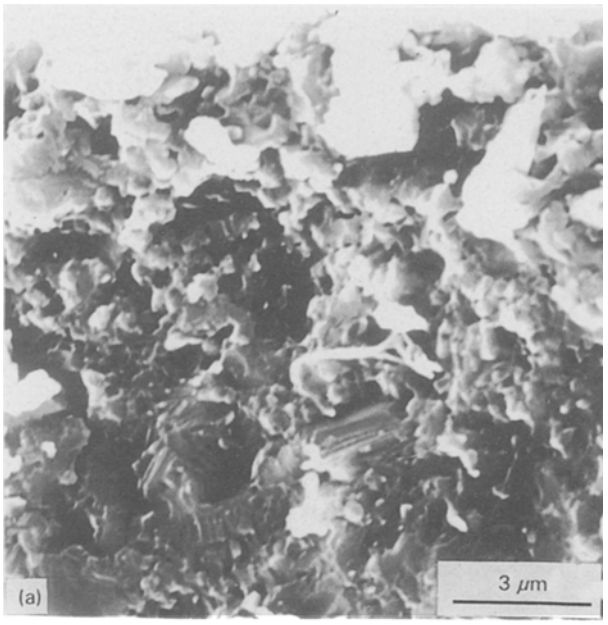

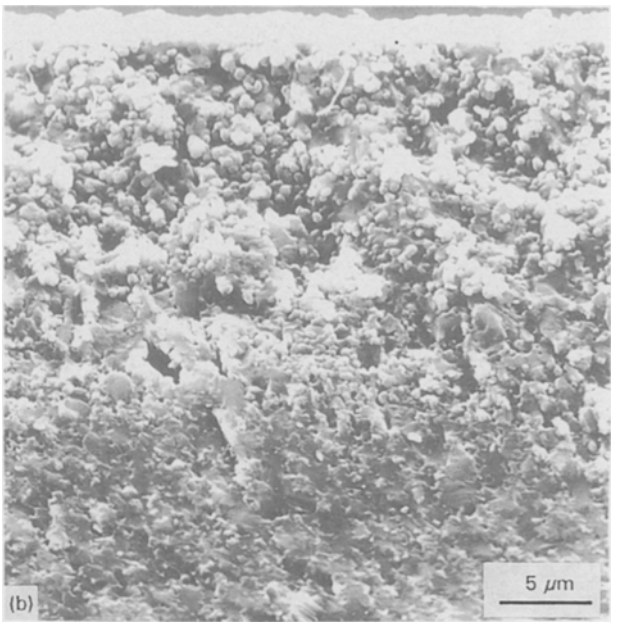

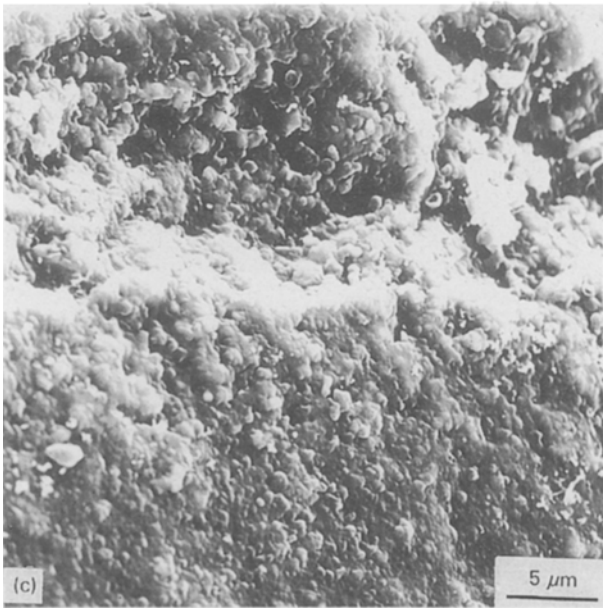

Figure 5 Scanning electron micrographs showing the fracture surfaces of the thermally aged nanocomposites at 1400 °C for (a) 8, (b) 40 and (c) 90 h.

ceramic, if the Al_2O_3–5.0 vol % SiC nanocomposite is simply regarded as a SiC ceramic containing an excess amount of Al_2O_3. For a given ageing duration, the surface scale formed in the nanocomposite investigated in the present work is much thicker than that formed in a polycrystalline SiC ceramic on ageing at 1400 °C in air [15]. The difference in the oxidation rate is related to the difference in microstructure between the two materials. The nature of the surface scale formed during thermal ageing is therefore different between the two materials. A continuous protection layer of amorphous silica formed on the oxidized surface is responsible for the lowered oxidation rate in the SiC ceramic. In contrast, SiC particles are a minor

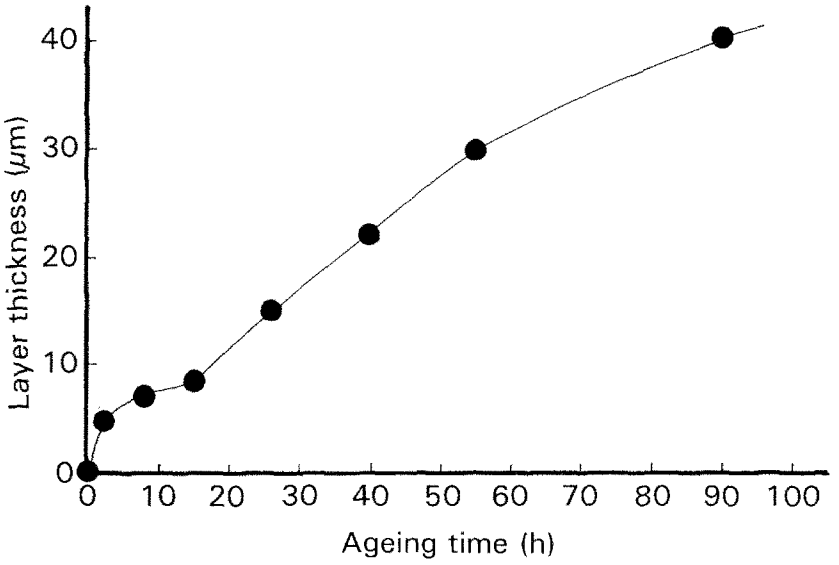

Figure 6 The relationship between the thickness of the reacted surface layer (scale) and the ageing time in the thermally aged nanocomposite at 1400 °C in air.

constituent (5 vol %), which does not form a continuous phase in the nanocomposite. The alumina grain boundaries will act as an easy path for the gaseous species and therefore oxidation proceeds from the SiC particles at the grain boundaries and grain junctions to those entrapped inside alumina grains. The resulting surface scale is discontinuous in nature, by inheriting grain boundaries from the polycrystalline Al_2O_3 matrix. These grain boundaries then function as a fast diffusion channel for the gaseous species across the surface scale, offering a low degree of protection for the nanocomposite inside from oxidation. The SiC particles in the nanocomposite are much smaller in size (20–30 nm) than the grains of conventional SiC ceramics and therefore are more susceptible to oxidation than the large SiC grains.

As shown in Fig. 6, the thickness of the surface scale increases with increasing ageing time. The increase rate would decrease with the increasing ageing time by following a single parabolic relationship between the scale thickness and ageing time, if no other physical and microstructural changes except the thickness increase took place within the surface scale [14]. Large microstructural defects, such as large cracks and/or crack-like pores, have been observed to occur in the surface scales, see Fig. 4a–d. There is no doubt that the oxidation of SiC particles and the subsequent reactions within the surface scales created new structural flaws. These microstructural defects will apparently facilitate the diffusion, both inward and outward, of gaseous species through the surface scale, leading to an increase in oxidation rate of the nanocomposite. This explains the pick-up in the increase rate of scale thickness at around 15 h in Fig. 6. As discussed earlier, the dispersion of SiC particles in the as-hot pressed nanocomposite was not uniform enough. SiC particle agglomerates of as large as 300 nm, within which little densification was achieved at the hot-pressing temperature, were shown to occur at the grain junctions of the alumina matrix. The porous SiC particle pockets are more susceptible to oxidation than the well-dispersed SiC particles entrapped within the alumina grains and may result in the formation of large microstructural defects in the oxidized surface scale. The residual microstructural defects present in the as-hot pressed nanocomposite, including the lamination cracks, pores and porous areas, may also result in the formation of large structural defects in the surface scale. They have a dramatic impact on the oxidation resistance of the nanocomposite. Fig. 7 is a scanning electron micrograph showing the fact that the surface scale formed around a large residual pore is thicker than that in the nearby regions where no large pores are present.

With increasing scale thickness at the ageing temperature, microstructural evolution takes place in the surface scale. This involves the reaction between silica and alumina and the grain growth of various phases. Therefore, the microstructure of the surface scale is strongly affected by the ageing time. Fig. 8a–d are bright-field transmission electron micrographs taken from the surface scale just behind the oxidation front in the nanocomposite aged at 1400 °C for 26 h. The

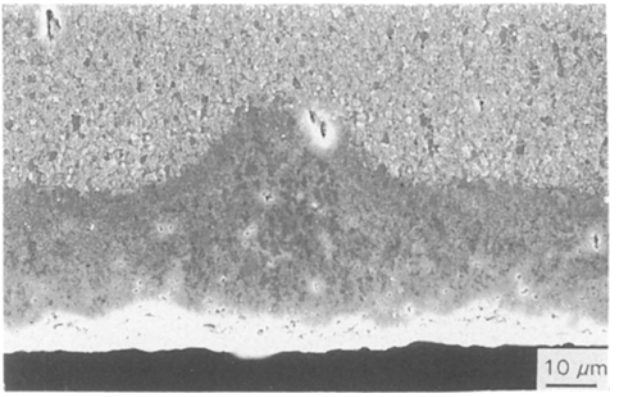

Figure 7 A scanning electron micrograph showing the effect of a large residual pore on the surface scale thickness in the nanocomposite thermally aged at 1400 °C for 55 h.

alumina matrix retained its original grain structures, although the SiC particles had completely disappeared. No unoxidized SiC particles and free carbon, which was observed to occur in SiC whisker-reinforced alumina composites when oxidized [17, 18], were found in this region. Both amorphous silica and aluminosilicates of differing composition were observed to occur at both intergranular and intragranular positions in the alumina matrix. The glassy aluminosilicate phases (up to 500 nm in size), which were an oxidation products of the SiC particle agglomerates in the as-hot pressed nanocomposite, were largely concentrated at the grain junctions. As discussed earlier, the conventional ball milling did not result in a high enough mixing homogeneity of the SiC particles in the alumina matrix. An estimated 20 % of the SiC particles, occurring mainly as particle agglomerates of 50–300 nm in size, were situated at the grain boundaries and grain junctions of the alumina matrix. The oxidation of these SiC agglomerates will apparently lead to the formation of large silica phases. Alumina content in these intergranularly positioned glass pockets varies considerably, from negligible amount up to that in stoichiometric mullite. Both small amorphous silica (30–60 nm) and large aluminosilicate pockets (100–200 nm) were found at the intragranular positions in the alumina matrix. They were oxidation products of the well-dispersed SiC particles entrapped within the alumina grains. Each SiC particle resulted in the formation of a small rounded amorphous silica phase when oxidized at the ageing temperature, although some SiC particles were oxidized prior to others. As shown in Fig. 8a and b, the intragranularly positioned aluminosilicate pockets exhibit a prismatic morphology, indicating that the amorphous silica dissolves the surrounding alumina grain at the ageing temperature. The co-existence of the small rounded amorphous silica and large prismatic aluminosilicate pockets within the same alumina grain is due to the fact that these micrographs were taken from the area just behind the oxidation front. The ageing time was not long enough for the rounded amorphous silica pockets to react with the alumina matrix and for mullite phases to precipitate out from the aluminosilicate pockets.

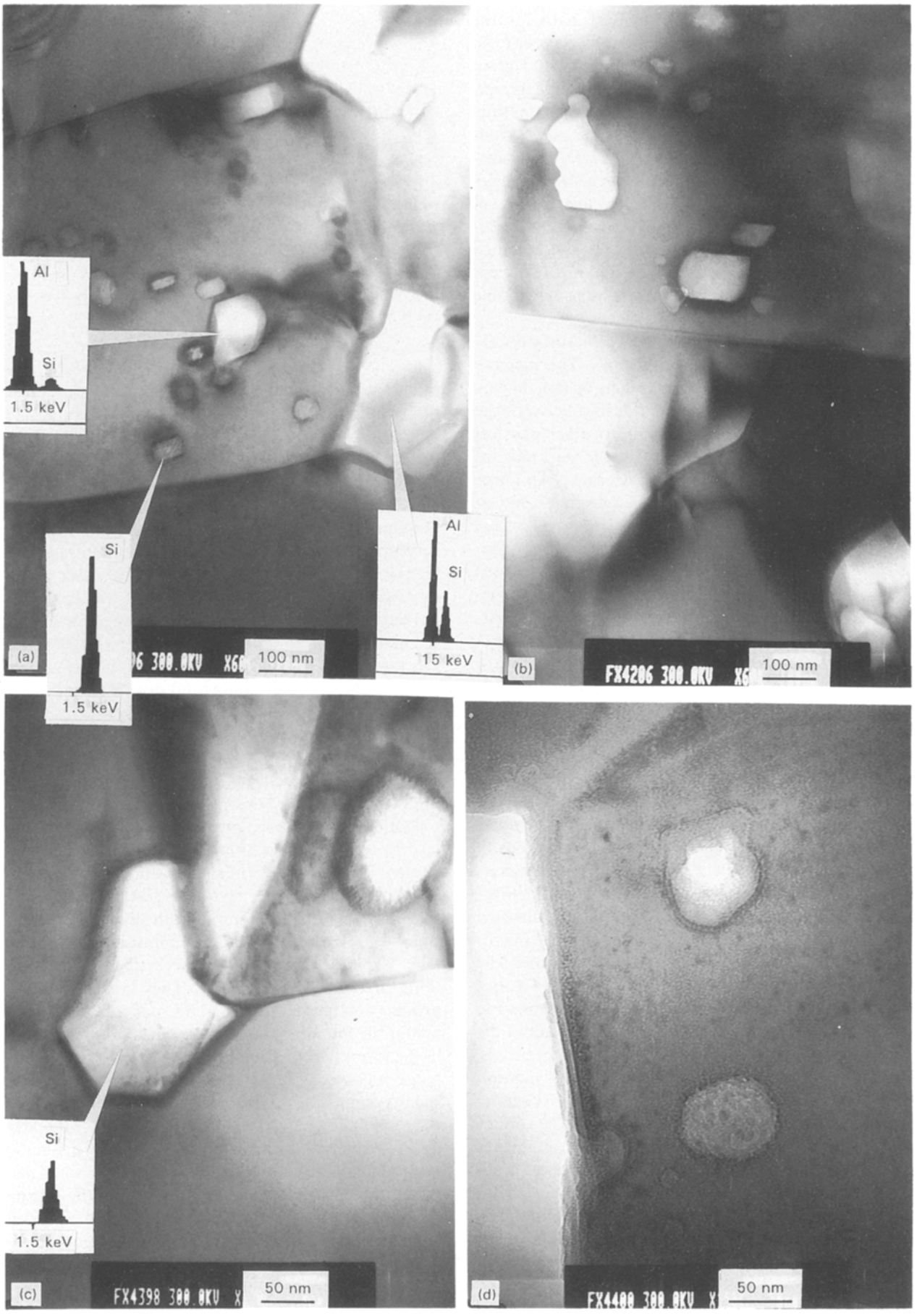

Figure 8 (a–d) Bright-field transmission electron micrographs showing the microstructure of the surface scale just behind the oxidation front in the nanocomposite aged at 1400 °C for 26 h. Both amorphous silica and aluminosilicate pockets were found to occur at the grain junctions and within alumina grains.

Phase equilibrium may never be reached in the surface scale, although a more complete reaction between the amorphous silica and the alumina matrix is expected when the nanocomposite is kept at the ageing temperature for a longer period. The situation is very similar to that in mullite ceramics prepared via reaction sintering or some sol–gel based processing routes [23–25]. There often exist grains of differing composition and/or differing morphology in each of these materials. Furthermore, amorphous silica and glassy aluminosilicate pockets, the composition of which may be approaching that of stoichiometric mullite, have been found to occur in many mullite ceramics. Fig. 9a and b are two bright-field micrographs taken from the surface scale approximately 30 μm from the oxidation front in the nanocomposite aged at 1400 °C for 90 h. It was estimated that the surface scale in this region was subjected to a thermal duration of > 60 h at the ageing temperature, following the completion of oxidation reaction at the reaction front. It is porous, consisting of large, irregularly shaped grains (up to 3 μm) and clusters of small equiaxial grains (submicrometre range). The grain structure of the alumina matrix, together with the SiC particles, have completely disappeared. Owing to the non-uniform distribution of SiC particles in the alumina matrix, the silica content varies considerably from one alumina grain to another and from one part of an alumina grain to another part of the same grain. The large, irregularly shaped grains were identified as mullite-type phases and exhibited compositions approaching that of stoichiometric mullite ($3Al_2O_3 \cdot 2SiO_2$), as indicated by EDX analysis. Dislocation networks and second-phase particles are observed to occur within them. The large sizes and irregular shapes are related to the rapid grain growth rate of mullite ceramics at 1400 °C. It is very probable, on the one hand, that some of the dislocation networks entrapped within these large mullite grains are inherited from the Al_2O_3 grains containing SiC particles in the as-hot pressed Al_2O_3–5.0 vol % SiC nanocomposite. As shown in Fig. 2a and b, many SiC-containing alumina grains exhibit a dislocation network. The dislocation structure within an alumina grain may not be necessarily eliminated during the oxidation of SiC particles and the subsequent reaction processes. On the other hand, new dislocation networks may be generated in the mullite grains at the thermal ageing temperature, where the grain growth rate of the mullite phase is high and certain second phase particles are engulfed by the fast growing mullite grains [26]. The small equiaxial grains were identified as alumina, the occurrence of which was a direct result of the non-uniform dispersion of SiC particles in the as-hot pressed nanocomposite.

The second-phase particles entrapped within the large, irregularly shaped mullite grains were identified as alumina and low silica-containing mullite, respectively, see Fig. 10a–d. The alumina particles tend to be more ellipsoidal and more irregular in shape and often

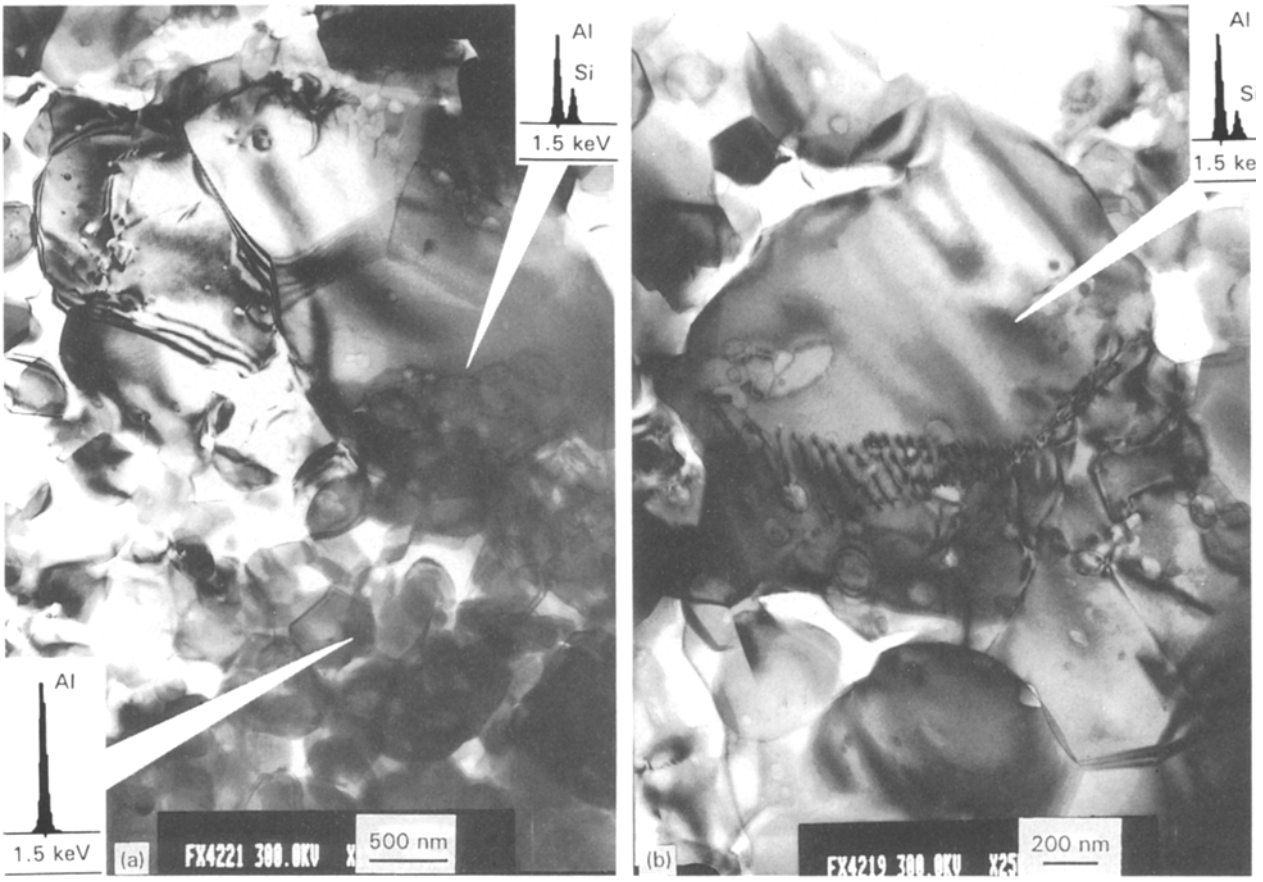

Figure 9 (a, b) Bright-field transmission electron micrographs showing the microstructure of surface scale approximately 30 μm from the oxidation front in the nanocomposite aged at 1400 °C for 90 h.

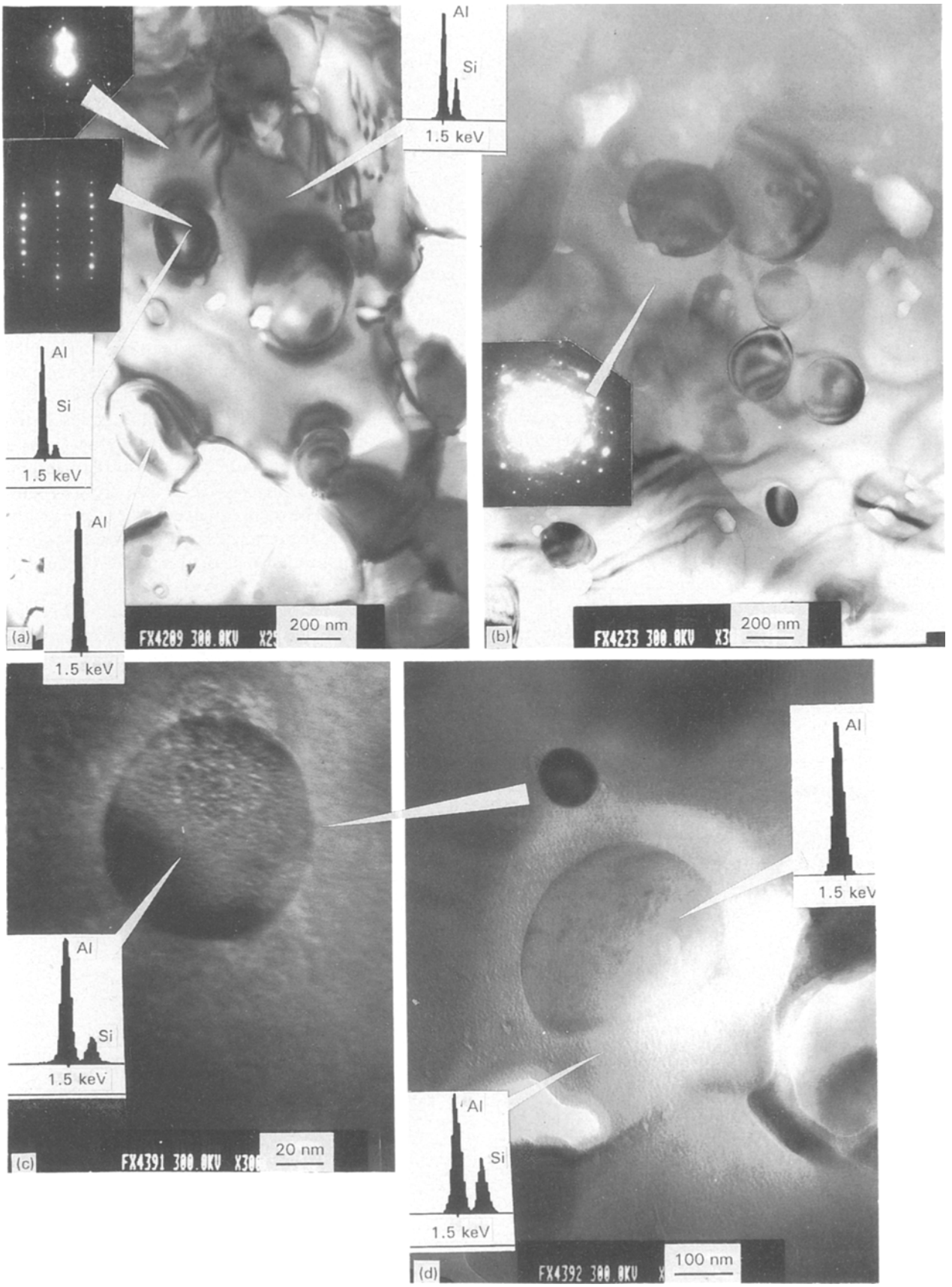

Figure 10 (a–d) Bright-field transmission electron micrographs and associated SAD patterns for the surface scale in the thermally aged nanocomposite at 1400 °C for 90 h. These micrographs show the occurrence of (i) rounded alumina particles at the grain junctions and within large mullite grains; and (ii) low silica-containing mullite particles (15 %–20 % silica) entrapped within the mullite matrix grains.

exhibit a slightly larger particle size than the mullite particles, although both exhibit a rounded morphology. It is considered that these two types of intragranularly positioned second phase particle have completely different origins. The alumina particles occur as being entrapped by the fast growing mullite grains at the thermal ageing temperature. They, as either an alumina grain or part of an alumina grain in most

cases, did not contain any SiC particles in the as-hot pressed nanocomposite. The oxidation and subsequent reactions in the nearby high SiC-containing regions resulted in the formation of mullite grains, which then swallowed up these silica-free areas. As has been established in mullite ceramics prepared by heating a diphasic Al_2O_3–SiO_2 precursor, the mullite matrix has potential to dissolve the engulfed alumina particles [27, 28]. The dissolution process continues until the alumina content in the mullite matrix is close to the highest tolerable amount at 1400 °C. Therefore, the particle size of the entrapped alumina particles decreases with increasing ageing time, and at the same time the alumina content in the mullite matrix increases. It is likely that many of the small alumina particles have disappeared completely into the large mullite grains. The ellipsoidal morphology of the alumina particle shown in Fig. 10d indicates that it was partially dissolved by the surrounding mullite matrix at the ageing temperature.

The occurrence of the low-silica containing mullite particles, as a second phase, in the large mullite grains is a result of the mullite formation via a dissolution and precipitation mechanism and subsequently being swallowed up by the high-silica containing mullite grains [29]. When oxidized, each well-dispersed SiC particle entrapped within an alumina grain results in the formation of a similarly sized amorphous silica pocket. The local mixing scale of homogeneity between the amorphous silica pocket and the surrounding alumina is in the nanometre range, although the alumina grain is large in size. This is similar to the mixing scale in diphasic Al_2O_3–SiO_2 precursors, prepared by certain sol–gel routes for mullite ceramics, such as by rapidly hydrolysing salt or alkoxide solutions [30, 31]. As has been established, mullitization in these diphasic precursors of nanometre scale mixing homogeneity occurs via a dissolution and precipitation mechanism, rather than as an interfacial reaction found in reaction-sintered mullite systems. Little mullitization takes place at temperatures below 1200 °C, although transitional phases such as γ-Al_2O_3 and spinel may form in the powder precursors over the temperature range 1000–1200 °C. At temperatures above 1200 °C, crystalline alumina or Al_2O_3-rich spinel is slowly dissolving in the amorphous silica. Mullite crystallites precipitate out from the siliceous amorphous matrix when the alumina content reaches the saturation concentration necessary to support mullite nucleation [29]. Continuous dissolution of the alumina or the spinel phase in the siliceous matrix leads to subsequent growth of the mullite precipitates. In the thermally aged Al_2O_3–SiC nanocomposite, dissolution of the alumina matrix grain into the intragranularly positioned amorphous silica phase, which is an oxidation product of the well-dispersed SiC particles, is clearly shown by the formation of prismatic aluminosilicate pockets in the alumina grains just behind the oxidation front, see Fig. 8a and b. The alumina content in each of these amorphous silica pockets increases as the dissolution of the alumina matrix continues at the ageing temperature. Mullite nuclei form and then grow when the alumina content exceeds the critical nucleation concentration for mullitization. The resulting mullite phases during this initial nucleation and subsequent growth period may exhibit a silica content approaching the high silica limit within the solid solution range of mullite [32]. However, the Al/Si ratio in these mullite particles increases when they dissolve the surrounding alumina matrix. Owing to the presence of excess alumina matrix, their compositions move toward the silica-deficient direction. EDX analysis indicated that the intragranularly positioned mullite particles exhibit a silica content of 14–20 wt %. This agrees well with the

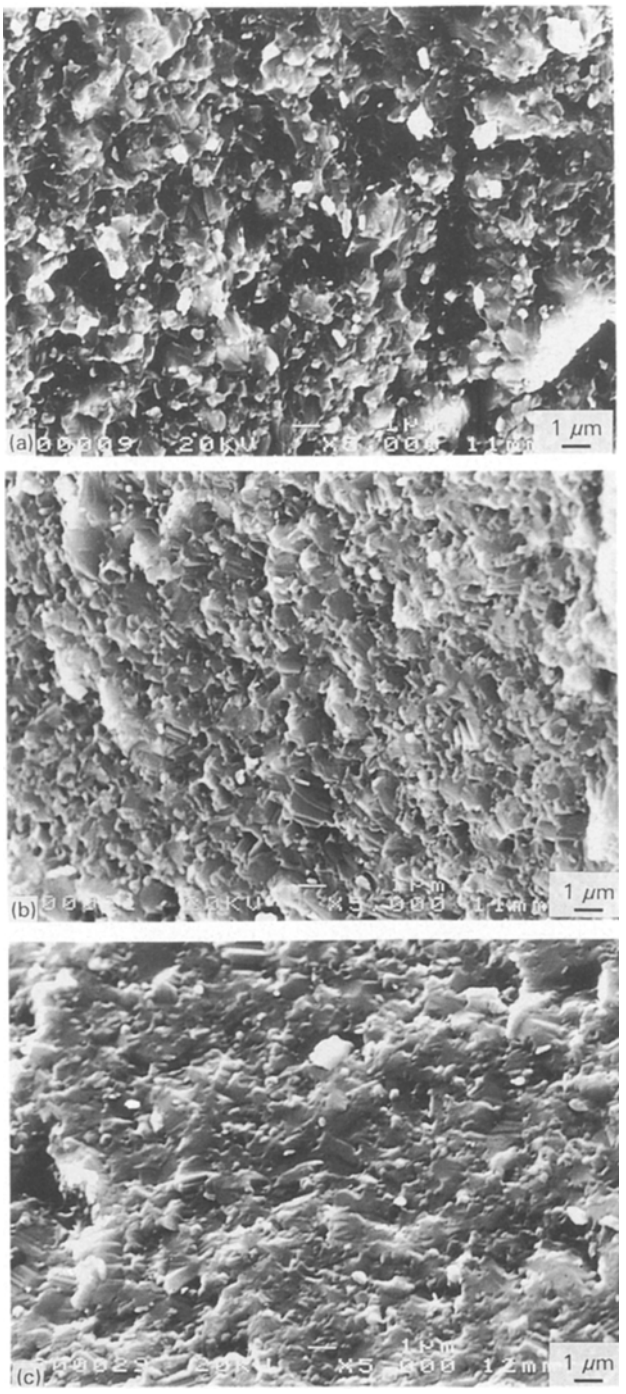

Figure 11 Scanning electron micrographs showing the fracture surfaces of the retained nanocomposites just ahead the oxidation front in the materials thermally aged at 1400 °C for (a) 8, (b) 55 and (c) 90 h, respectively. They all demonstrate a mainly transgranular fracture surface.

experimental results of Aksay and Pask [32], Kriven and Pask [33] and Li and Thomson [28], who observed that the bottom limit of silica content in metastable mullite is 16.4 wt % at temperatures below 1450 °C. As discussed above, the oxidation and subsequent reactions in the high SiC-containing areas, either as a SiC particle agglomerate or as an alumina grain or part of an alumina grain containing a high density of well-dispersed SiC particles, result in the formation of the high silica-containing mullite grains. These matrix mullite grains undergo a dramatic grain growth at the ageing temperature, engulfing both the small alumina particles and the low-silica containing mullite precipitates.

Finally, very little difference was found in microstructure between the retained nanocomposite in the bulk region of the thermally aged samples and the unaged nanocomposite. Fig. 11a–c are scanning electron micrographs showing the fracture surfaces of the retained nanocomposites just ahead the oxidation front in the samples thermally aged at 1400 °C for 8, 55 and 90 h. They all demonstrate a mainly transgranular fracture surface, which is exactly the same as the fracture surface for the unaged nanocomposite, see Fig. 3. As expected, SiC particles in these bulk regions were not oxidized. Fig. 12 is a bright-field transmission electron micrograph showing the microstructure of the retained nanocomposite in the material thermally aged at 1400 °C for 90 h. The only difference between the thermally aged nanocomposite and the unaged nanocomposite, see Fig. 2a and b, is that the average grain size of the alumina matrix in the former

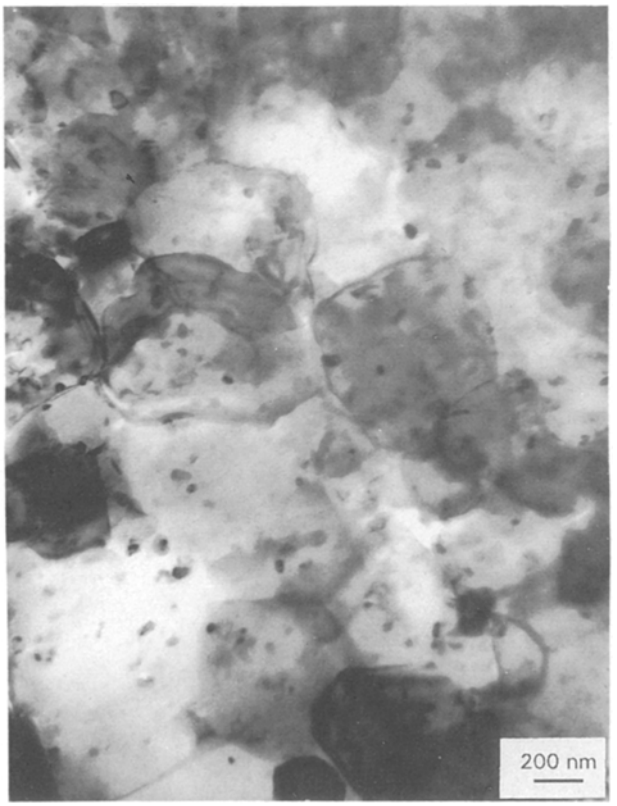

Figure 12 A transmission electron micrograph showing the microstructure of the bulk nanocomposite in the material thermally aged at 1400 °C for 90 h.

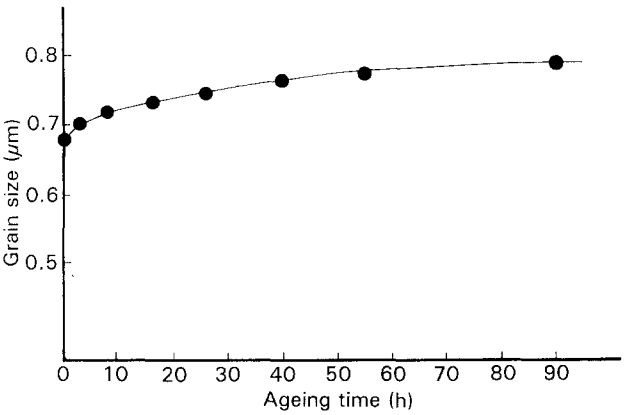

Figure 13 The average grain size of the alumina matrix in bulk nanocomposite dotted against ageing time at 1400 °C.

is slightly larger than that in the latter. As shown in Fig. 13, the average grain size of the alumina matrix increases only slightly with increasing ageing time at 1400 °C. This implies that the Al_2O_3–SiC nanocomposite exhibits a stable microstructure against thermal ageing as far as the SiC particles are effectively protected from oxidation. Apparently, the SiC particles play a critical role in inhibiting grain growth of the alumina matrix at the thermal ageing temperature.

4. Conclusion

The microstructural stability of an alumina nanocomposite containing 5.0 vol % SiC, which was fabricated via a hot-pressing route using submicrometre alumina and silicon carbide powders as the starting materials, has been studied by thermally ageing the as-hot pressed nanocomposite in air for various periods at 1400 °C. The thermal treatment leads to the formation of a surface scale, the thickness of which increases with increasing ageing time at the ageing temperature. SiC particles within the surface scale are oxidized to form silica, which subsequently reacts with the alumina matrix. The surface scale exhibits a porous microstructure, consisting of alumina grains, mullites of differing composition, and amorphous silica and silicate pockets. Two types of mullite phase, which contain a high and a low level of silica, respectively, have been identified in the surface scales. Owing to the non-uniform distribution of SiC particles in the alumina matrix, mullitization mechanisms operating in the surface scales at the ageing temperature include both interfacial reaction and dissolution and precipitation. The low-silica containing mullite particles are observed to occur as a second-phase particle entrapped within the large, irregularly shaped matrix mullite grains, which exhibit a composition close to that of stoichiometric mullite. The former was formed via a dissolution and precipitation mechanism and was subsequently swallowed up by the fast growing matrix mullite grains. The microstructure in the bulk region of the thermally aged nanocomposite remains almost intact when compared with that of the unaged nanocomposite. The only noticeable difference is that the grain size of the alumina matrix in the thermally aged nanocomposite is slightly larger than that in the unaged nanocomposite.

Acknowledgements

The authors thank Robert Condor for fabricating the hot-pressed nanocomposite used in the present investigation and the SERC for financial support during the period of this work.

References

1. A. SAWAGUCHI, K. TODA and K. NIIHARA, *J. Ceram. Soc. Jpn* **99** (1991) 510.
2. K. NIIHARA and A. NAKAHIRA, in "Proceedings of 3rd International Symposium on Ceramic Materials Composites for Engines", edited by V. J. Tennery (The American Ceramic Society, Westerville, OH, 1988, pp. 919–26.
3. J. ZHAO, L. C. STEARNS, M. P. HARMER, H. M. CHEN and G. A. MILLER, *J. Am. Ceram. Soc.* **76** (1993) 503.
4. K. NIIHARA and A. NAKAHIRA, in "Advanced Structural Inorganic Composites" edited by P. Vincenzini (Elsevier Scientific, Trieste, 1990, pp. 637–64.
5. K. NIIHARA, *J. Ceram. Soc. Jpn* **99** (1991) 974.
6. A. BENNETT, *Mater. Sci. Technol.* **2** (1986) 895.
7. K. S. CHAN and R. A. PAGE, *J. Am. Ceram. Soc.* **76** (1993) 803.
8. N. S. JACOBSON, *ibid.* **76** (1993) 3.
9. G. ERVIN Jr, *ibid.* **44** (1958) 347–52.
10. J. A. COSTELLO and R. E. TRESSLER, *ibid.* **64** (1981) 327.
11. T. NARUSHIMA, T. GOTO and T. HIRAI, *ibid.* **72** (1989) 1386.
12. J. W. HINZE and H. C. GRAHAM, *J. Electrochem. Soc.* **123** (1976) 1066.
13. R. R. SICKAFOOSE Jr and D. W. READEY, *J. Am. Ceram. Soc.* **76** (1993) 316.
14. B. E. DEAL and A. S. GROVE, *J. Appl. Phys.* **36** (1965) 3770.
15. J. A. COSTELLO and R. E. TRESSLER, *J. Am. Ceram. Soc.* **69** (1986) 674.
16. S. C. SINGHAL and F. F. LANGE, *ibid.* **58** (1975) 433.
17. W. M. KRIVEN, G. VAN TENDELOO, T. N. TIEGS and P. F. BECHER, in "Materials Science Research, Vol. 21, Ceramic Microstructure'86", edited by J. A. Pask and A. G. Evans (Plenum Press, New York, 1987) pp. 939–47.
18. M. B. RICOULT, *J. Am. Ceram. Soc.* **74** (1991) 1793.
19. K. L. LUTHRA and H. D. PARK, *ibid.* **73** (1990) 1014.
20. K. L. LUTHRA, *ibid.* **71** (1988) 1114.
21. M. MAEDA, K. NAKAMURA, T. OHKUBO, J. ITO and E. ISHII, *Ceram. Int.* **15** (1989) 247.
22. J. A. COSTELLO, R. E. TRESSLER and I. S. T. TSONG; *J. Am. Ceram. Soc.* **64** (1981) 332.
23. J. A. PASK, X. W. ZHANG, A. P. TOMSIA and B. E. YOLDAS, *ibid.* **70** (1987) 704.
24. M. N. RAHAMAN, L. C. DE JONGHE, S. L. SHINDE and P. H. TEWARI, *ibid.* **71** (1988) C-338.
25. J. MA RINCON, G. THOMAS and J. S. MOYA, *ibid.* **69** (1986) C-31.
26. M. D. SACKS, H. W. LEE and J. A. PASK, in "Ceramic Transactions", Vol. 6 "Mullite and Mullite Matrix Composites", edited by S. Somiya, R. F. Davis and J. A. Pask (American Ceramic Society, Westerville, OH, 1990) pp. 167–207.
27. J. C. HULING and G. L. MESSING, *J. Am. Ceram. Soc.* **72** (1989) 1725.
28. D. L. LI and W. J. THOMSON, *ibid.* **74** (1991) 2382.
29. S. SUNDARESON and I. A. AKSAY, *ibid.* **74** (1991) 2388.
30. W. C. WEI and J. W. HALLORAN, *ibid.* **71** (1988) 166.
31. I. A. AKSAY, D. M. DABBS and M. SARIKAYA, *ibid.* **74** (1991) 2343.
32. I. A. AKSAY and J. A. PASK, *ibid.* **58** (1975) 507–512.
33. W. M. KRIVEN and J. A. PASK, *ibid.* **66** (1983) 649.

Received 10 May
and accepted 9 June 1994